arXiv:1201.4046v1 [astro-ph.CO] 19 Jan 2012

Mon. Not. R. Astron. Soc. **000**, 1–10 (0000) Printed 20 January 2012 (MN LaTeX style file v2.2)

X-rays as dominant excitation mechanism of [Fe II] and H_2 emission lines in active galaxies

Oli L. Dors Jr.[1]⋆, Rogemar A. Riffel[2], Mónica V. Cardaci[3,4,5], Guillermo F. Hägele[3,4,5],
Ângela C. Krabbe[1], Enrique Pérez-Montero[6], Irapuan Rodrigues[1]
[1] *Universidade do Vale do Paraíba, Av. Shishima Hifumi, 2911, Cep 12244-000, São José dos Campos, SP, Brazil*
[2] *Universidade Federal de Santa Maria, Av. Roraima, 1000, Cep 97105-900, Santa Maria, Brazil*
[3] *Consejo Nacional de Investigaciones Científicas y Técnicas (CONICET), Argentina.*
[4] *Facultad de Ciencias Astronómicas y Geofísicas, Universidad Nacional de la La Plata, Paseo del Bosque s/n, 1900 La Plata, Argentina.*
[5] *Departamento de Física Teórica, C-XI, Universidad Autónoma de Madrid, 28049 Madrid, Spain.*
[6] *Instituto de Astrofísica de Andalucía (CSIC), PO Box 3004, 18080 Granada, Spain*

20 January 2012

ABSTRACT

We investigate the excitation mechanisms of near-infrared [Fe II] and H_2 emission lines observed in Active Galactic Nuclei (AGNs). We built a photoionization model grid considering a two-component continuum, one accounts for the Big Bump component peaking at 1Ryd and another represents the X-ray source that dominates the continuum emission at high energies. Photoionization models considering as ionizing source a spectral energy distribution obtained from photometric data of the Sy 2 Mrk 1066 taken from the literature were considered. Results of these models were compared with a large sample of observational long-slit and Integral field Unit (IFU) spectroscopy data of the nuclear region for a sample of active objects. We found that the correlation between the observational [Fe II]$\lambda1.2570\,\mu$m/Paβ vs. $H_2\lambda2.1218\,\mu$m/Brγ is well reproduced by our models as well as the relationships that involve the H_2 emission line ratios observed in the spectroscopic data. We conclude that the heating by X-rays produced by active nuclei can be considered a common and very important mechanism of excitation of [Fe II] and H_2.

Key words: galaxies: Seyfert – galaxies: ISM – infrared: galaxies

1 INTRODUCTION

The excitation of the Narrow Line Region of Seyfert (Sy) galaxies can reveal how radiation and mass outflows from the nucleus interact with circumnuclear gas. In particular, near-infrared (hereafter near-IR) observations are a powerful tool to investigate this issue, because the obscuration –which can affect the optical morphology of the emitting gas region– is less important at these wavelengths (Mulchaey et al. 1996; Ferruit et al. 2000). Relevant emission-lines in the near-IR include [Fe II] $\lambda\,1.2570\,\mu$m and $\lambda\,1.6440\,\mu$m, H I lines such as Paβ, and H_2 at $\lambda\,1.9576\,\mu$m, $\lambda\,2.1218\,\mu$m, and $\lambda\,2.3085\,\mu$m, which can be used to map the gas kinematics and excitation (e.g. Riffel & Storchi-Bergmann 2011b; Riffel et al. 2010). Nevertheless, the dominant excitation mechanisms of the [Fe II] and H_2 emission lines in the central regions of active galaxies are still unclear and have been the subject of several recent studies (e.g. Riffel et al. 2010, 2008, 2006; Storchi-Bergmann et al. 2009; Hicks et al. 2009; Müller Sánchez et al. 2009; Ramos Almeida et al. 2009; Rodríguez-Ardila et al. 2005, 2004; Davies et al. 2007).

The H_2 can be excited by two mechanisms: (i) fluorescent excitation through absorption of soft-UV photons (912–1108 Å) in the Lyman and Werner bands, existing both in star-forming regions and surrounding the Active Galactic Nuclei (AGNs) (Black & van Dishoeck 1987) and (ii) collisional excitation due to the heating of the gas by shocks, the interaction of a radio jet with the interstellar medium (Hollenbach & McKee 1989), or by X-ray photons from the central AGN (Maloney et al. 1996). Several studies based on intensity-line ratios (Riffel et al. 2010; Storchi-Bergmann et al. 2009; Rodríguez-Ardila et al. 2005, 2004) have shown that collisional excitation processes dominate the H_2 emission surrounding AGNs. However, which is the dominant process is an open question. Veilleux et al. (1997), using J and K-band spectra of a sample of 33 Sy 2 galaxies, found that shocks associated with nuclear outflows are a likely source of both [Fe II] and H_2 emission rather than circumnuclear starbursts, as suggested by Quillen et al. (1999).

For the [Fe II] emission, the [Fe II] $\lambda\,1.2570\,\mu$m/Paβ line ratio is generally used to investigate the main mechanism of excitation.

⋆ E-mail:olidors@univap.br

The value of this line ratio is controlled by the quotient of the volumes of partially and fully ionized gas regions, with [Fe II] emission being excited in the partially ionized gas (Mouri et al. 1990, 1993; Rodríguez-Ardila et al. 2005; Riffel et al. 2010, 2008, 2006; Storchi-Bergmann et al. 2009). Such zones in AGNs are created by X-ray emission (e.g. Simpson et al. 1996) and/or shock heating of the gas by mass outflows from the nuclei which interact with the ambient clouds (e.g. Forbes & Ward 1993). This problem was addressed by Mouri et al. (2000), who compared the values of the line ratios [Fe II] λ 1.2570 μm/Paβ and [O I] λ 6300 Å/Hβ predicted by models, considering photoionization and shock heating, with those observed in a sample of AGNs and Starburst galaxies. These authors pointed out that in AGNs, X-ray heating is the most important [Fe II] excitation mechanism. However, Rodríguez-Ardila et al. (2004), using near-IR spectroscopy of a sample of galaxies obtained with the Infrared Telescope Facility, found that X-ray excitation is enough to explain the H_2 emission and part of the [Fe II] emission observed in Sy 1 galaxies, but fails to explain the emission of these elements in Sy 2. For these objects, a combination of shocks and circumnuclear starformation is required to explain these emissions. Moreover, it is not clear whether the [Fe II] and H_2 are excited by the same mechanism. Rodríguez-Ardila et al. (2004) found a correlation between the [Fe II] λ 1.2570 μm/Paβ and the H_2 λ 2.1218 μm/Brγ ratios, indicating that both sets of lines may be originated by a single dominant mechanism. However, high spatial resolution spectroscopy data from Integral Field Unit (IFU) of active galaxies indicate that the H_2 and the [Fe II] emitting gas have distinct flux distributions and kinematics, with the former being considered a tracer of the feeding of the AGN and the latter a tracer of its feedback (Riffel et al. 2010, 2009, 2008; Storchi-Bergmann et al. 2009; Hicks et al. 2009; Müller Sánchez et al. 2009). This result indicates that the lines of these elements are formed in distinct regions. Although several works have investigated the excitation origins of H_2 and the [Fe II], it is still unknown whether a common mechanism can excite these elements. Fortunately, a large number of near-IR data of AGNs are currently available in the literature, which enables an extensive comparison with models yielding a more reliable conclusion about the likely dominant excitation mechanism of these emission lines.

In this paper, we combined near-IR data of Sy galaxies obtained with IFU and long-slit spectroscopy with photoionization models to investigate the origin of the H_2 and [Fe II]. In Section 2, we describe the observational data used in the analysis. The modelling procedures are presented in Sect. 3. In Sect. 4, the diagnostic diagrams used to compare the observational data with our model predictions are described. Results and discussion are presented in Sects. 5 and 6, respectively. A conclusion of the outcome is given in Sect. 7.

2 OBSERVATIONAL DATA

We compiled from the literature observational data of the nuclear region of active galaxies in the near-IR and optical spectral range obtained with long-slit and IFU spectroscopy. The selection criterion was the presence of bright infrared emission lines in their spectra. These data are described below.

2.1 Long-slit data

Near-IR emission line intensity ratios of 35 active galaxies were obtained from Rodríguez-Ardila et al. (2004), Reunanen et al. (2002), Knop et al. (2001), and Riffel et al. (2006). This sample comprises long-slit data of 13 Sy 1 and 21 Sy 2 galaxies, along with 1 Quasar. The intensities of the near-IR [Fe II] and H_2 emission lines observed in these objects were compared with our photoionization models. We also used the [O III] λ 5007 Å/Hβ and [O I] λ 6300 Å/Hα line intensity ratios of about 600 000 emission-line galaxies listed in the MPA/JHU Data catalogue of the Sloan Digital Sky Survey DR7 release (available at http://www.mpa-garching.mpg.de/SDSS/DR7/).

2.2 IFU data

For this study we selected two Sy 1 galaxies, Mrk 1157 and NGC 4151, and two Sy 2 galaxies (ESO 428-G14 and Mrk 1066). All of them were previously observed by our group using the IFU spectrographs of the Gemini telescopes. We selected these objects because both J- and K-band spectroscopic data are available. The observations of Mrk 1066, Mrk 1157, and NGC 4151 were performed using the Near-IR Integral field Spectrograph (NIFS; McGregor et al. 2003) on Gemini North, while ESO 428-G14 was observed with the Gemini Near Infra-Red Spectrograph (GNIRS; Elias et al. 1998) on Gemini South.

3 PHOTOIONIZATION MODEL

To analyse the [Fe II] and H_2 excitation mechanisms, we built a grid of models using the photoionization code Cloudy/08 (Ferland et al. 1998), and then we compared the line intensity ratios predicted by them with those observed. The spectral energy distribution (SED) of the ionizing source used as input for the Cloudy code was a two-component continuum ranging from $\sim 10^{15}$ Hz to $\sim 10^{21}$ Hz. The shape of this SED is similar to the one observed in typical AGNs for that range. The first is the Big Bump component peaking at 1 Ryd with a high-energy and an infrared exponential cutoff and the second one represents the X-ray source that dominates at high energies and is characterized by a power law with an index $\alpha_x = -1$. Its normalization was computed to produce the required value of the optical to X-ray spectral index α_{ox}. This index describes the continuum between 2 keV and 2500 Å (Zamorani et al. 1981). We assumed the default value of the Cloudy code $\alpha_{ox} = -1.4$, because that is about the average of the observed values, which are between -1.0 and -2.0, for the entire range of observed luminosities of AGNs (Miller et al. 2011; Zamorani et al. 1981).

The cosmic ray emission was considered in the models as a second ionizing source. Cosmic rays heat the ionized gas and produce secondary ionizations in the neutral gas, which mostly increase the intensities of the H_2 emission lines. We assumed a value of the H_2 ionization rate of 10^{-15} s^{-1}, which is about the same rate found by McCall et al. (2003) for a galactic line of sight. It is worth noting that the value of the cosmic ray rate must be estimated object by object. For example, Suchkov et al. (1993) found for M 82 a cosmic ray rate several times larger than the one in the Milk Way. Gamma ray observations of the starburst NGC 253 by Acero et al. (2009) indicate a cosmic ray rate three orders of magnitude larger than that for the Milky Way. Also, molecular data of star forming galaxies, such as Arp 220, show evidence for extremely high cosmic ray rates yielded by the UV emission from supernova remnants (Meijerink et al. 2011).

We computed a sequence of models assuming an electron density $N_e = 10^4$ cm^{-3}, ionization parameter U in the range $-4.0 \leqslant \log U \leqslant -1.0$ defined as $U = Q_{ion}/4\pi R_S^2 nc$, where Q_{ion} is the number of hydrogen ionizing photons emitted per second by

Table 1. Fe/O and O/H gas phase abundances assumed in the models.

Metallicity ($Z/Z_\odot$)	12+log(O/H)	log(Fe/O)		
2	9.0	-1.47(a1)	-1.94(a2)	-2.24(a3)
1	8.69	-1.77(b1)	-2.24(b2)	-2.77(b3)
0.5	8.38	-2.15(c1)	-2.54(c2)	-2.76(c3)

the ionizing source, R_S is the Strömgren radius (in cm), n is the particle density (in cm^{-3}), and c is the speed of light. The chosen range of these values for U is typical of narrow-line regions of Sy galaxies (e.g. Ferland & Netzer 1983). The H_2 emission lines are very dependent on the electron density value assumed in the models. For example, when N_e varies from 10^3 to 10^5 cm^{-3}, the logarithm of the $H_2\,\lambda\,2.1218\,\mu$m/Br$\gamma$ emission line intensity ratio span about 2.6 dex. The value $N_e = 10^4 cm^{-3}$, assumed in our models, is a mean value from those considered by Mouri et al. (2000). We considered in our models three values of 12+log(O/H)= 8.38, 8.69, and 9.00, which correspond to values of the metallicity 0.5, 1, and 2 times the solar value published by Allende Prieto et al. (2001). The abundances of other metals in the nebula were scaled linearly to the solar metal composition through the comparison of the oxygen abundances, with the exception of the N and Fe abundances. The nitrogen abundance was taken from the relation log(N/O)=log(0.034+120O/H) of Vila- Costas & Edmunds (1993). The Fe/O abundance ratio has a large scatter for a fixed O/H value (Izotov et al. 2006) and its value is uncertain because the Fe and O abundances in grains are poorly known (Peimbert & Peimbert 2010). Thus, we varied the Fe/O abundance ratio by about 0.7 dex on each metallicity.

The presence of internal dust was considered and the grain abundances (van Hoof et al. 2001) were also linearly scaled with the oxygen abundance. To take into account the depletion of refractory elements onto dust grains, the abundances of Mg, Al, Ca, Ni, and Na were reduced by a factor of 10, and Si by a factor of 2 relative to adopted abundances in each model in accordance with Garnett et al. (1995). In Table 1, the O/H and Fe/O abundance values of the gas phase assumed in the models are shown. The model of the H_2 molecule described by Shaw et al. (2005) and the model of the Fe^+ ion described by Verner et al. (1999), which consider 371 energy levels, were assumed in our computations. The outer radius of the modelled nebula is that where the temperature falls below 1000 K.

4 DIAGNOSTIC DIAGRAMS

We used four diagnostic diagrams containing predicted and observed emission line ratios of the [Fe II] , H_2, [O III], and [O I] which are described below.

- [Fe II] $\lambda\,1.2570\,\mu$m/Paβ vs. $H_2\,\lambda\,2.1218\,\mu$m/Br$\gamma$ (Fig. 1) — Diagnostic diagram suggested by Larkin et al. (1998) and Rodríguez-Ardila et al. (2004) to separate galaxies according to their level of nuclear activity. Recently, Riffel et al. (2010) constructed this diagram with spatially resolved IFU data of an AGN. Typical values for the nucleus of Sy galaxies are 0.6 $\lesssim$ [Fe II] $\lambda\,1.2570\,\mu$m/Pa$\beta \lesssim$ 2.0 and 0.6 $\lesssim H_2\,\lambda\,2.1218\,\mu$m/Br$\gamma \lesssim$ 2.0 (Rodríguez-Ardila et al. 2005). This [Fe II]/Paβ is very dependent on the Fe/O abundance while the H_2 emission lines are dependent on the ionization parameter.
- $H_2\lambda\,1.957\,\mu$m/$\lambda\,2.121\,\mu$m and $H_2\lambda\,2.033\,\mu$m/$\lambda\,2.223\,\mu$m vs. $H_2\lambda\,2.247\,\mu$m/$\lambda\,2.121\,\mu$m (Fig. 2) — Mouri (1994) proposed these diagrams to separate gas emission yielded by shocks from emission caused by fluorescence. The drawback in using the $H_2\lambda\,1.957\,\mu$m/$\lambda\,2.121\,\mu$m ratio is that the $H_2\lambda\,1.957\,\mu$m may be affected by telluric bands of H_2O and CO_2, or blended with the [Si IV] $\lambda\,1.963\,\mu$m emission line (Rodríguez-Ardila et al. 2005).

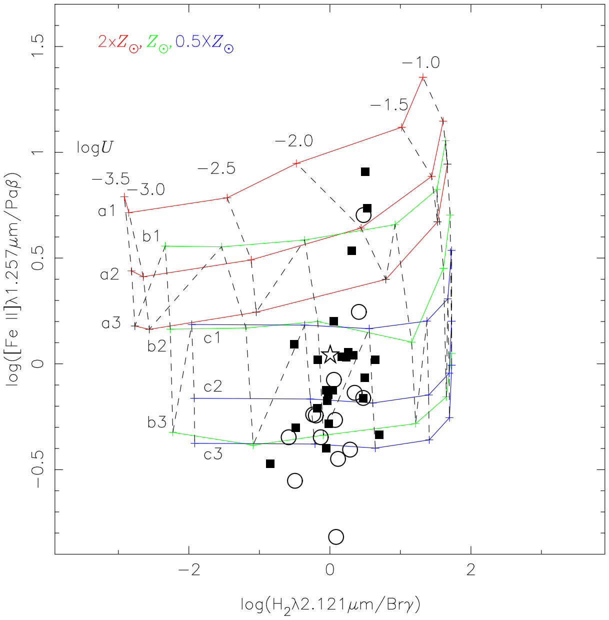

Figure 1. Diagnostic diagram showing the observational data taken from the literature (see Sect. 2) and results from the grid of photoionization models (see Sect.3). Solid lines connect curves of iso-Z, while dotted lines connect curves of iso-U. The values of $\log U$ and Z are indicated. The three different lines for each Z correspond to the different assumed values of the Fe/O as indicated by the labels (see Table 1). Circles, squares, and star represent Sy1, Sy2, and quasar data, respectively. The typical error bar (not shown) of the emission line ratios is about 10 %.

- [O III] $\lambda\,5007$Å/Hβ vs. [O I] $\lambda\,6300$Å/Hα (Fig. 3) — This diagram was suggested by Baldwin et al. (1981) to separate objects according to their primary excitation mechanisms, i.e. (a) photoionization by stars, (b) photoionization by a power law continuum source or (c) shock heating. In particular, the [O I] $\lambda\,6300$ Å/Hα line ratio is greatly increased by the presence of shocking gas, even when it has low velocities (e.g. Allen et al. 2008).

5 RESULTS

5.1 Integrated spectra

In Figs. 1 and 2 we show the first three diagnostic diagrams described above containing the results of our grid of photoionization models and the data sample. Sy 1, Sy 2 and quasar are represented by different symbols. For the IFU data, the emission line ratios represented in these Figs. were estimated by integrating the spaxels inside a central aperture of 0.5″×0.5″ for each galaxy, with exception of ESO428-G14 for which an aperture of 0.75″×0.75″ was considered. These values are presented in Table 2.

In Fig. 1, we can see that almost all the observational ratios are within the parameter space defined by our grid of photoionization models. A lower metallicity than those assumed in our models is required to reproduce the data of the galaxies out of the grid. The observed correlation between [Fe II] $\lambda\,1.2570\,\mu$m/Paβ and

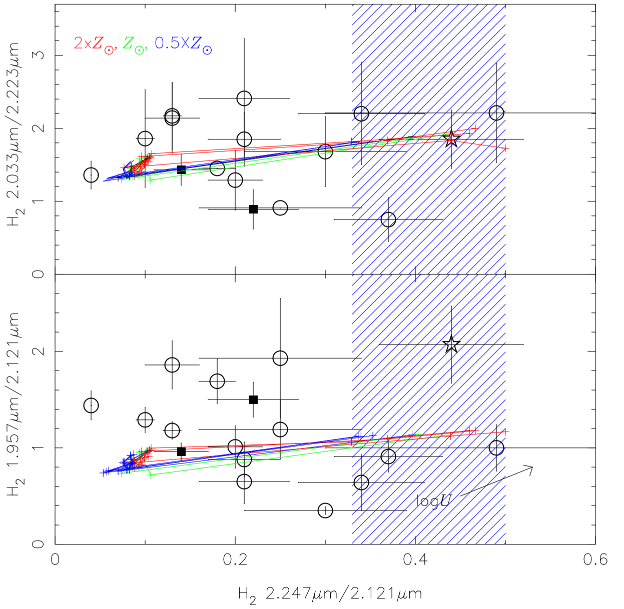

Figure 2. As in Fig. 1 for H_2 emission lines. The arrow indicates the direction in which the ionization parameter increases. Circles, squares, and star represent Sy1, Sy2, and quasar data, respectively. The hatched area represents the region occupied by shock model results from Hollenbach & McKee (1989).

Table 2. Integrated line ratio intensities of IFU data

Object	[Fe II] $\lambda\,1.2570\,\mu$m/Paβ	H_2 $\lambda\,2.1218\,\mu$m/Brγ
ESO428-G14	0.75	1.10
Mrk 1066	0.52	0.96
Mrk1 157	0.73	2.24
NGC 4151	0.45	0.26

H_2 $\lambda\,2.1218\,\mu$m/Brγ is explained by an increase in metallicity and ionization parameter. Noteworthy that the parameter space defined by the models built using $Z = 0.5\,Z_\odot$ is almost completely contained in the one defined by the models built using the solar metallicity.

In the case of the diagnostic diagrams that only involve H_2 line ratios (Fig. 2), the photoionization models are slightly dependent on the assumed metallicities, covering almost the same parameter space, and strongly dependent on variations in the ionization parameter. Taking into account the observational error bars, our models are in good agreement with the observed $H_2\lambda\,2.033\,\mu$m/$\lambda\,2.223\,\mu$m and $H_2\lambda\,2.247\,\mu$m/$\lambda\,2.121\,\mu$m ratios (upper panel). On the other hand, in the lower panel of Fig. 2 can be noticed larger dispersion of the observational data which is not well reproduce by the models. This dispersion could be the result of a contamination of the measurements of the H_2 $\lambda\,1.957\,\mu$m emission line intensities due to a blend with the [Si IV] $\lambda\,1.963\,\mu$m line (as explained above). Therefore, the predicted $H_2\lambda 1.957\,\mu$m intensities are somewhat lower than the observed ones. In Fig. 2, we also show the area occupied by the theoretical intensities of the line ratio $H_2\lambda\,2.247\,\mu$m/$\lambda\,2.121\,\mu$m from shock models performed by Hollenbach & McKee (1989). These authors computed emission-line spectra of steady interstellar shocks in molecular gas considering velocities from 30 to 150 km/s and particle densities of $10^3 - 10^6$ cm^{-3}. We can see that most of the objects of our sample appear to have the X-rays as main ionizing source while for the remaining ones a composite ionization by X-rays and shock can be considered.

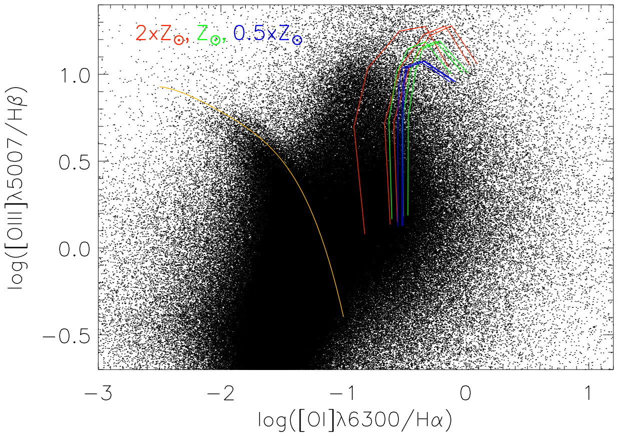

Figure 3. [O III] $\lambda\,5007$ Å/Hβ vs. [O I $\lambda\,6300$ Å/Hα diagnostic diagram. The yellow line separates objects ionized by massive stars from those containing active nucleus (Kewley et al. 2001). Blue, green and red solid lines are as in Fig. 1. Points represent emission-line galaxies listed in the MPA/JHU Data catalogue of the Sloan Digital Sky Survey DR7 release (see Sect. 2).

Fig. 3 shows the [O III] $\lambda\,5007$ Å/Hβ vs. [O I $\lambda\,6300$ Å/Hα diagnostic diagram. In this Fig. we can see that the observational data of AGNs are well describe by our models. If our models use the lower values of the ionization parameter ($\log U < -3.5$; these models are not shown), we can extend the parameter space to include the objects that have values of the logarithm of the [O III] $\lambda\,5007$ Å/Hβ ratio lower than zero. As in the case of the [Fe II] $\lambda\,1.2570\,\mu$m/Paβ and H_2 $\lambda\,2.1218\,\mu$m/Brγ diagnostic diagram (Fig. 1), the parameter space of the models with solar metallicity almost contains that of the $Z = 0.5\,Z_\odot$ models.

5.2 IFU data

We plot the [Fe II] $\lambda\,1.2570\,\mu$m/Paβ and H_2 $\lambda\,2.1218\,\mu$m/Brγ diagnostic diagram for each spaxel of our four objects with our model results (see upper panels of Figs. 4 and 5). In these Figs., the spaxel data are separated by their ionization mechanism according to the place in the diagnostic diagram, with different colours for each mechanism. The different ionization mechanism zones are delimited in the Figs. by dashed-lines, following the work of Rodríguez-Ardila et al. (2004). The spaxels showing typical values of starbursts, Seyferts, and low-ionization nuclear emission-line regions (LINERs) are represented by green open circles, black filled circles, and red crosses, respectively. With the same colour code, we show the spatial position of each spaxel in the IFU field of view (see lower panels of Figs. 4 and 5). Our models completely represent the region occupied by Seyfert and LINERs data.

6 DISCUSSION

The excitation mechanism of the near-IR emission lines of the [Fe II] and H_2 in active galaxies have been the subject of several works. For example, Mouri et al. (2000) compared results of models considering photoionization by X-rays and shock heating

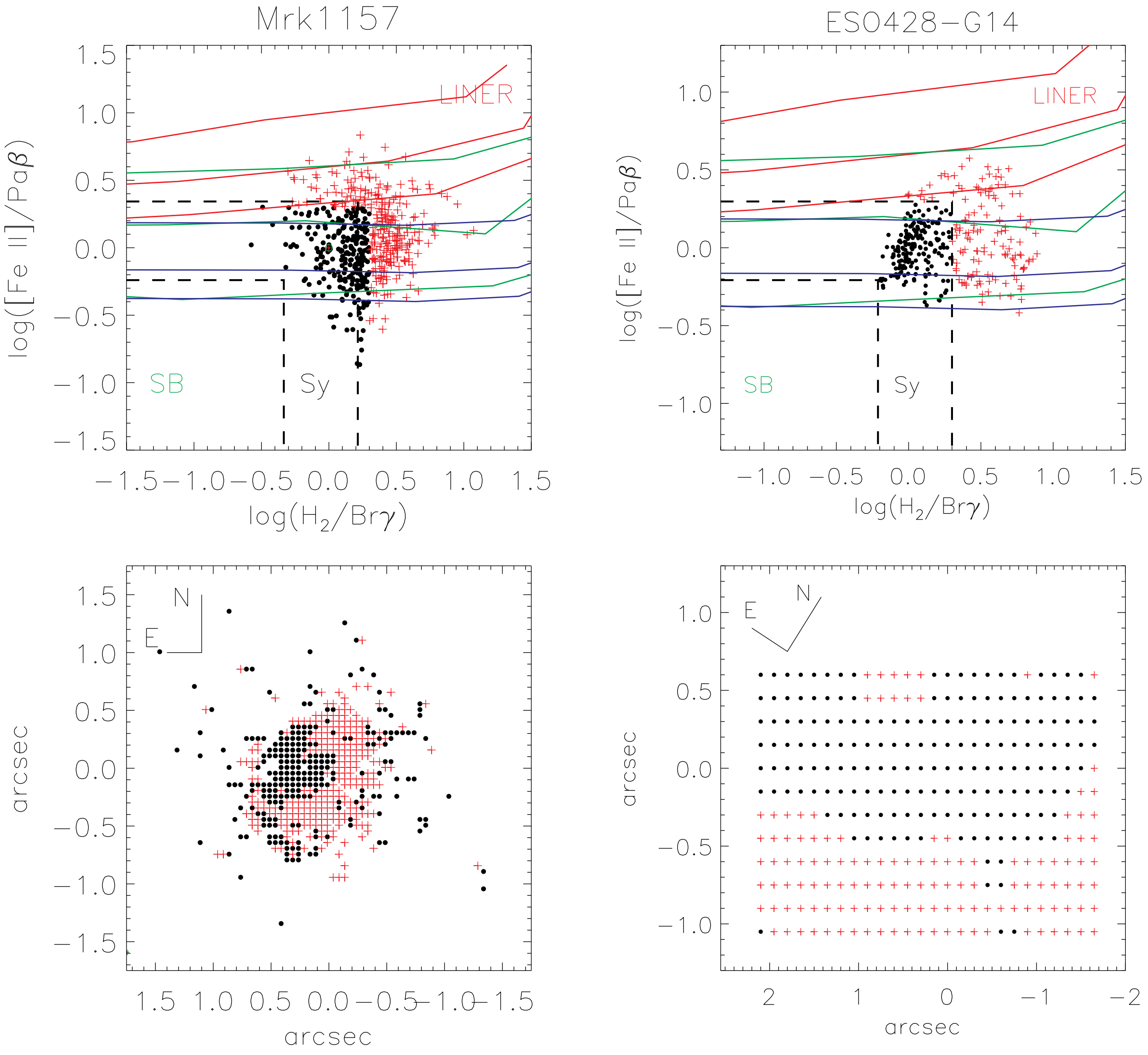

Figure 4. Top panels: [Fe ii] λ 1.2570 μm/Paβ vs. H_2 λ 2.1212 μm/Brγ line-ratio diagnostic diagram for Mrk 1157 (left) and ESO 428-G14 (right). The dashed lines delimit regions with ratios typical of Starbursts (green open circles), Seyferts (black filled circles) and LINERs (red crosses). Blue, green and red solid lines are as in Fig. 1. Bottom panels: spatial position of each spaxel in the IFU field of view from the diagnostic diagram.

with observational data of AGNs and starburst galaxies. These authors built their models considering large ranges in shock velocities, gas density, metallicity, and different ionizing continua. Mouri and collaborators showed that the [Fe ii] emission is enhanced when a partially ionized zone is produced by photoionization by X-rays (described by a power-law) and shock heating. These two processes can be discriminated by the electron temperature of the [Fe ii] region: 8000 K in heating by X-rays and 6000 K in shock heating. Comparing the electron temperature of the [Fe ii] region estimated by Thompson (1995) for NGC 4151 ($8000 < T_e < 12000$ K) with their models, Mouri et al. (2000) showed that, at least for this galaxy, it indicates that X-rays are the more important mechanism to yield the [Fe ii] flux. These authors arrived to the same conclusion using the [O i] λ 6300 Å/Hα vs. [Fe ii]λ1.2570 μm]/Paβ diagnostic diagram. A similar result was also obtained by Jackson & Beswick (2007) by analysing J-band spectra of three Sy 2 galaxies.

For our models, we assumed an incident continuum whose shape is given by two components, a Big Bump and an X-ray power law, varying the Fe/O abundance. With these models that do not consider shock heating, we are able to explain the observational data. Nevertheless, we do not exclude some contribution by shock heating to the [Fe ii] emission. Comparing our models with the SDSS DR7 emission-line galaxies (Fig. 3), we are able to describe the [O i]/Hα line ratio observed in AGNs. This diagram cannot be used to discriminate [Fe ii] excitation mechanism, nevertheless, we must take into account that the [O i]/Hα line ratio is shock sensitive. Hence, although shock contribution in the ionization of Fe cannot be ruled out, models considering a continuum described by a Big Bump and an X-ray power law as the ionization source can also reproduce the [Fe ii] emission lines as well as the behaviour of shock sensitive emission lines such as [O i] λ 6300 Å. Analysing IFU observations of the Sy galaxy NGC 4151, Turner et al. (2002) found that the [Fe ii] emission mainly arises in the visible narrow-line re-

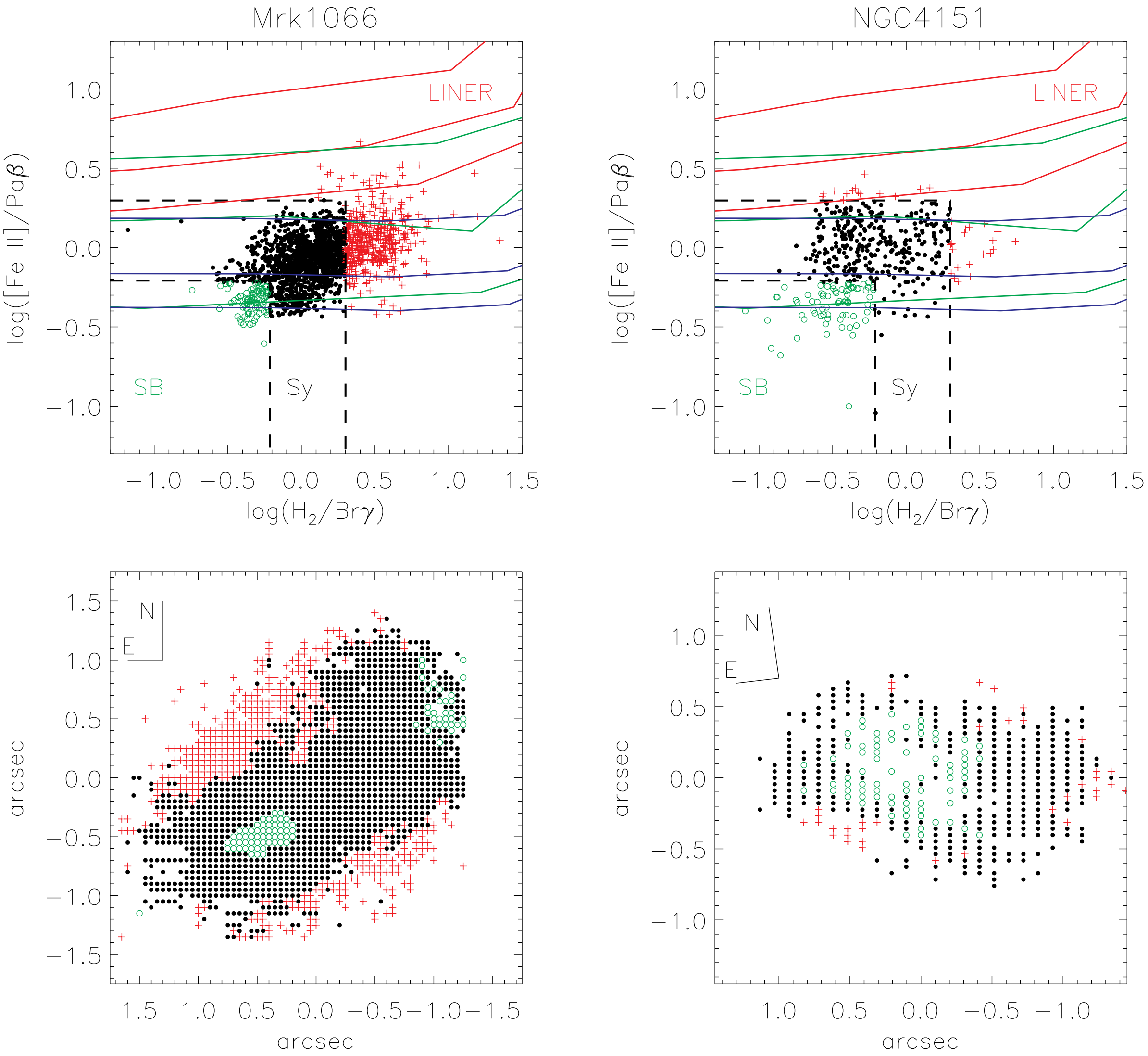

Figure 5. As in Fig. 4 but for Mrk 1066 (left) and NGC 4151 (right).

gion in which the dominant excitation mechanism is the photoionization by collimated X-ray emission from the nucleus. Oliva et al. (2001) pointed out that in regions where shocks are the dominant mechanism the iron-based grains are destroyed but the phosphorus is not, yielding a larger [Fe II] $\lambda\,1.2570\,\mu$m/[P II] $\lambda\,1.188\,\mu$m line-ratio intensity than that observed in the regions dominated by X-ray. In order to verify this, in Fig. 6 we show a histogram containing this observed line intensity ratio for 17 Seyfert galaxies, 5 Sy 1 and 12 Sy 2, taken from Jackson & Beswick (2007), Riffel et al. (2006), and Oliva et al. (2001). It can be seen that the [Fe II]/[P II] for Sy galaxies ranges from 1.5 to 6 (with a mean value of 2.7). The mean value of this ratio is about 20 for SNRs, which indicate that the emitting gas has recently passed through a fast shock (Oliva et al. 2001). Therefore, these results confirm that shocks have little influence on the [Fe II] emission.

Regarding the H_2, this molecule can be excited via three distinct mechanisms: (1) UV fluorescence, where photons with $\lambda > 912$ Å are absorbed by the H_2 molecule and then re-emitted, resulting in the population of various vibro-rotational levels, (2) shocks, where high-velocity gas motions heat and accelerate this molecule; and (3) X-ray illumination, where hard X-ray photons penetrate deep into molecular clouds, heating large amounts of molecular gas resulting in the H_2 emission (see Rodríguez-Ardila et al. 2004, and references therein). Rodríguez-Ardila and collaborators used the diagrams shown in Fig. 2 to compare observational data of 22 objects with models considering a thermal emission, a non-thermal UV excitation, a thermal UV excitation, and a mixture of thermal and low-density fluorescence. These authors found that for 4 objects the excitation mechanism is clearly thermal, while for the remaining objects a mixing with a non-thermal process cannot be discarded, even though the results point out to a dominant thermal mechanism.

To analyse the relative weight of the X-ray emission with respect to the other model components (mainly with fluorescence and UV photons), not only for the H_2 emission but also for the [Fe II], we made models fixing all parameters with the exception of the α_{ox} value (see Fig. 7), which is related to the X-ray power law normalization (see Section §3). We assumed $Z = Z_\odot$ and $\log U = -2.5$

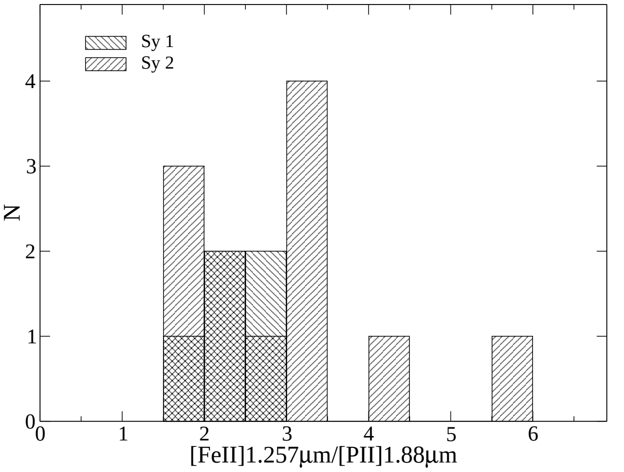

Figure 6. Histogram showing the [Fe II]/[P II] emission line intensity ratios of a sample of objects collected from the literature.

since the models built using the solar metallicity and this value of the ionization parameter cover almost all the parameter space occupied by the observational data (see Fig. 1). Taking into account the α_{ox} definition (Tananbaum et al. 1979), which fixes the Big Bump parameters, a decrement of the α_{ox} value implies that the amount of the X-rays emitted by the source decreases. In Fig. 7 we can see that our models with $\alpha_{ox} = -1.4$ reproduce well the observational AGN data. Nevertheless, when we use lower values of this parameter, the ratios predicted by the models go out of the region typically occupied by the AGNs (Rodríguez-Ardila et al. 2004). Therefore, our models favour the scenario suggested by Maloney et al. (1996), where the H_2 molecule emission is mainly governed by photons emitted at X-ray wavelengths from the central AGN. This also can be inferred from the dependence of the H_2 emission lines on the ionization parameter U.

To verify if shock models can fit the observational data, we compared shock model results by Hollenbach & McKee (1989) with our sample (see Fig. 2). Only few observational points are located in the area occupied by these shock models and, even in these cases, models considering X-rays also describe the data.

On the other hand, varying in our models the H_2 ionization rate by cosmic rays by a factor of 200, we found that the $H_2\,\lambda\,2.1218\,\mu$m/Br$\gamma$ line ratio only increases by about 0.15 dex, which shows that the additional ionization by cosmic rays has little influence on the H_2 emission lines.

A simple scenario where both [Fe II] and H_2 emissions are mainly due to the X-ray continuum coming from the active nucleus has also been proposed by other authors. For example, Blietz et al. (1994) and Knop et al. (2001) showed that X-rays from the nucleus can heat the gas located in the narrow line region driving the [Fe II] and H_2 emission. Because 98 % of the iron is tied up in dust grains, this process must free the iron through dust destruction and yet not destroy the H_2 molecules (Rodríguez-Ardila et al. 2004). These authors computed the emergent [Fe II] $\lambda\,1.2570\,\mu$m and $H_2\,\lambda\,2.1218\,\mu$m flux using the X-ray models by Maloney et al. (1996) and compared their predictions with observational data of seven objects. They found that X-ray heating can only explain a fraction of the [Fe II] and H_2 emission, and they stated that the discrepancy found can be alleviated if the emitting gas is located closer than the distance adopted in their models. The X-ray data, provided by the *XMM-Newton* and *Chandra* space telescopes, and their detailed analysis (see e.g. Piconcelli et al. 2005; Longinotti et al. 2007; Bianchi et al. 2009; Krongold et al. 2009; Cardaci et al. 2011; Corral et al. 2011, and references therein), provide information about the continuum shape and the particular spectral features of the AGNs in this wavelength range. For Mrk 1066, we compared the results obtained using this simple scenario that only involves a continuum modelled by a Big Bump and an X-ray power law with those obtained using its intrinsic SED. We built the observational SED taking the photometric data from the NASA/IPAC Extragalactic Database (NED), following

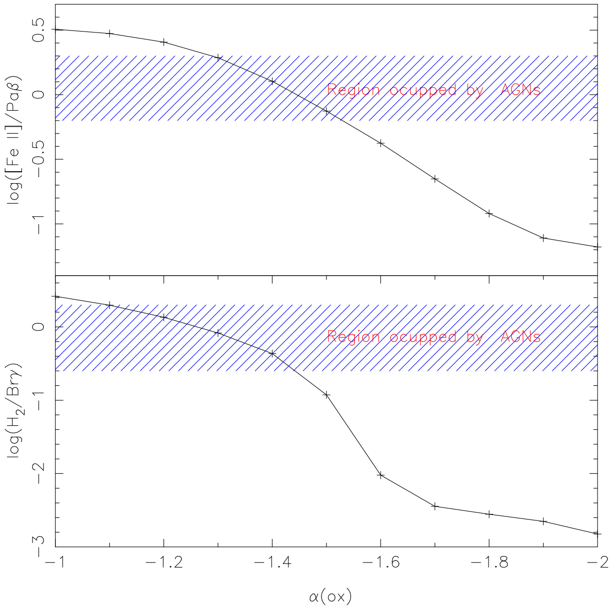

Figure 7. Model results using solar metallicity, $N_e = 10^4$ cm^{-3}, log U = -2.5 and varying only the α_{ox} parameter to see the influence of the X-rays on the [Fe II] $\lambda\,1.2570\,\mu$m/Paβ and $H_2\,\lambda\,2.1218\,\mu$m/Br$\gamma$ emission line ratios. To delimit the region occupied by the AGNs we follow Rodríguez-Ardila et al. (2004).

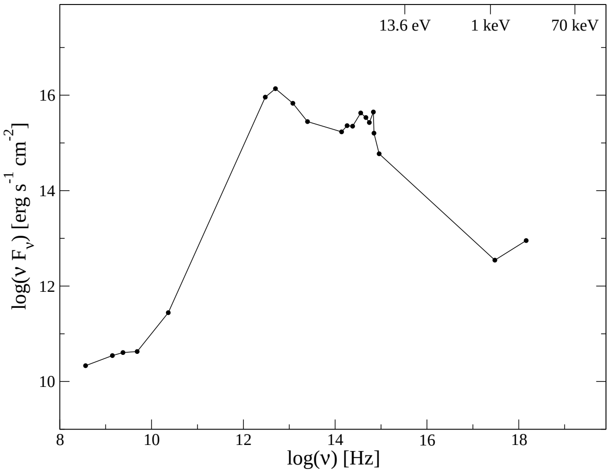

Figure 8. Spectral energy distribution at the Schwarzschild radio (10^{-5} pc) of the Sy 1 galaxy Mrk 1066 used as the photoionization source for some models of this galaxy. We assumed a galaxy distance of 50 Mpc (Mould et al. 2000). The photometric data were taken from Dressel & Condon (1978), Moshir et al. (1990), de Vaucouleurs et al. (1991), Becker et al. (1991), Douglas et al. (1996), Condon et al. (2002), Skrutskie et al. (2003), Braatz et al. (2004), Guainazzi et al. (2005), Muñoz-Marín et al. (2007), and Cardamone et al. (2007).

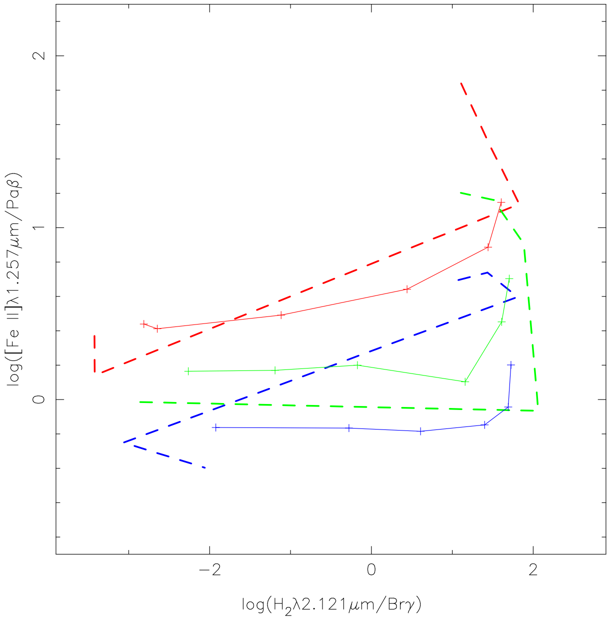

Figure 9. Comparison between the grid model results shown in Fig. 1 (solid lines) and the models built considering the semi-empirical SED of Mrk 1066 shown in Fig. 8 (dashed lines).

Cardaci et al. (2009). To enhance the number of points of the SED as needed by Cloudy, we performed a linear interpolation among the semi-empirical points (see Fig. 8). We built a new grid of photoionization models under the same assumptions of abundances, ionization parameters and density, but only for one value of the Fe/O ratio for each metallicity. In Fig. 9 the predictions of our models using the SED of Mrk 1066 and the model results presented in Fig. 1 assuming the same Fe/O abundance as the Mrk 1066 models are shown. The model results derived using the two different ionizing sources are mostly in agreement.

The semi-empirical SED of Mrk 1066 includes not only the range covered by the Cloudy model but also the radio and IR wavelengths. Hence, the agreement between solid and dashed lines in Fig. 9 only indicates that the assumed multicomponent model is a good representation of the AGN continuum when studying the [Fe II] and H_2 emission.

Recent resolved integral field spectroscopy of the central region of active galaxies shows that the ionized (in particular the [Fe II] emitting gas) and the molecular (traced by the H_2 emission) gas have distinct flux distributions and kinematics. The molecular component is more restricted to the plane of the galaxies and the ionized one extends to high latitudes above it, which is in most cases co-spatially with the radio jet (e.g., Riffel et al. 2006, 2008, 2009, 2010; Riffel & Storchi-Bergmann 2011a,b; Storchi-Bergmann et al. 2009, 2010). Usually the [Fe II] has an enhancement in flux and velocity dispersion in regions surrounding the radio structure, suggesting that the radio jet plays an important role in the [Fe II] emission. Our models are able to reproduce the [Fe II] emission of active galaxies without considering shock excitation by the radio jet. Thus, the enhancement in the [Fe II] flux in the vicinity of radio structures can be interpreted as being due to an enhancement in the gas density, caused by the interaction of the radio jet with the emitting gas, and mainly excited by X-rays from the central engine.

The main exciting mechanism of infrared emission lines of ESO 428-G14, Mrk 1157, Mrk 1066 and NGC 4151 was discussed by Riffel et al. (2006, 2008, 2010) and Storchi-Bergmann et al. (2009), respectively. However, these authors did not reach conclusive results. For example, Riffel et al. (2006) suggested that the [Fe II] excitation in ESO 428-G14 is mainly due to shocks. Nevertheless, the detailed analysis performed in the present work confronting our models with the IFU data shows that X-rays are a more reliable dominant excitation mechanism even in the case of ESO 428-G14.

7 CONCLUSIONS

In this work we show that a photoionization model grid built by adopting a continuum source characterized by two components, one accounting for the Big Bump component peaking at 1 Ryd and the other describing the X-rays emission, is able to reproduce the [Fe II] and H_2 infrared emission lines of a sample of AGNs. Testing the influence of the X-rays on the intensity of these emission lines, we found that a decrement in the X-ray content of the continuum source translates into a weakening of these lines, and the models are no longer compatible with the observations. This implies that the heating by the X-ray emission from the active nuclei can be considered as the most important mechanism of excitation for the IR emission lines of these elements.

ACKNOWLEDGMENTS

We are grateful to the referee, Neal Jackson, for a thorough reading of the manuscript and for suggestions that greatly improved its clarity.

Based on observations obtained at the Gemini Observatory, which is operated by the Association of Universities for Research in Astronomy, Inc., under a cooperative agreement with the NSF on behalf of the Gemini partnership: the National Science Foundation (United States), the Science and Technology Facilities Council (United Kingdom), the National Research Council (Canada), CONICYT (Chile), the Australian Research Council (Australia), Ministério da Ciência e Tecnologia (Brazil) and south-eastCYT (Argentina). This research has made use of the NASA/IPAC Extragalactic Database (NED) which is operated by the Jet Propulsion Laboratory, California Institute of Technology, under contract with the National Aeronautics and Space Administration. OLD and ACK are grateful to the FAPESP for support under grant 2009/14787-7 and 2010/01490-3. MC and GH are grateful to the Spanish Ministerio de Ciencia e Innovación for support under grant AYA2010-21887-C04-03, and the Comunidad de Madrid under grant S2009/ESP-1496 (ASTROMADRID). EPM is grateful to the Spanish Ministerio de Ciencia e Innovación for support under grant AYA2010-21887-C04-02, and the Junta de Andalucía under grant TIC114.

REFERENCES

Acero F., Aharonian F., Akhperjanian A. G., Anton G., Barres de Almeida U., Bazer-Bachi A. R., Becherini Y., Behera B., Bernlöhr K., Bochow A., and 160 coauthors, 2009, Science, 326, 1080

Allen M. G., Groves B. A., Dopita M. A., Sutherland R. S., Kewley L. J., 2008, Astrophys. J., Suppl. Ser., 178, 20

Allende Prieto C., Lambert D. L., Asplund M., 2001, Astrophys. J. Letters, 556, L63

Baldwin J. A., Phillips M. M., Terlevich R., 1981, Publ. Astron. Soc. Pac., 93, 5

Becker R. H., White R. L., Edwards A. L., 1991, Astrophys. J., Suppl. Ser., 75, 1

Bianchi S., Guainazzi M., Matt G., Fonseca Bonilla N., Ponti G., 2009, Astron. Astrophys., 495, 421

Black J. H., van Dishoeck E. F., 1987, Astrophys. J., 322, 412

Blietz M., Cameron M., Drapatz S., Genzel R., Krabbe A., van der Werf P., Sternberg A., Ward M., 1994, Astrophys. J., 421, 92

Braatz J. A., Henkel C., Greenhill L. J., Moran J. M., Wilson A. S., 2004, Astrophys. J. Letters, 617, L29

Cardaci M. V., Santos-Lleó M., Hägele G. F., Krongold Y., Díaz A. I., Rodríguez-Pascual P., 2011, Astron. Astrophys., 530, A125+

Cardaci M. V., Santos-Lleó M., Krongold Y., Hägele G. F., Díaz A. I., Rodríguez-Pascual P., 2009, Astron. Astrophys., 505, 541

Cardamone C. N., Moran E. C., Kay L. E., 2007, Astron. J., 134, 1263

Condon J. J., Cotton W. D., Broderick J. J., 2002, Astron. J., 124, 675

Corral A., Della Ceca R., Caccianiga A., Severgnini P., Brunner H., Carrera F. J., Page M. J., Schwope A. D., 2011, Astron. Astrophys., 530, A42+

Davies R. I., Müller Sánchez F., Genzel R., Tacconi L. J., Hicks E. K. S., Friedrich S., Sternberg A., 2007, Astrophys. J., 671, 1388

de Vaucouleurs G., de Vaucouleurs A., Corwin Jr. H. G., Buta R. J., Paturel G., Fouque P., 1991, Third Reference Catalogue of Bright Galaxies. Volume 1-3, XII, 2069 pp. 7 figs.. Springer-Verlag Berlin Heidelberg New York

Douglas J. N., Bash F. N., Bozyan F. A., Torrence G. W., Wolfe C., 1996, Astron. J., 111, 1945

Dressel L. L., Condon J. J., 1978, Astrophys. J., Suppl. Ser., 36, 53

Elias J. H., Vukobratovich D., Andrew J. R., Cho M. K., Cuberly R. W., Don K., Gerzoff A., Harmer C. F., Harris D., Heynssens J. B., Hicks J., Kovacs A., Li C., Liang M., Moon I. K., Pearson E. T., Plum G., Roddier N. A., Tvedt J., Wolff R. J., Wong W.-Y., 1998, in A. M. Fowler ed., Society of Photo-Optical Instrumentation Engineers (SPIE) Conference Series Vol. 3354 of Society of Photo-Optical Instrumentation Engineers (SPIE) Conference Series, Design of the Gemini near-infrared spectrometer. pp 555–565

Ferland G. J., Korista K. T., Verner D. A., Ferguson J. W., Kingdon J. B., Verner E. M., 1998, Publ. Astron. Soc. Pac., 110, 761

Ferland G. J., Netzer H., 1983, Astrophys. J., 264, 105

Ferruit P., Wilson A. S., Mulchaey J., 2000, Astrophys. J., Suppl. Ser., 128, 139

Forbes D. A., Ward M. J., 1993, Astrophys. J., 416, 150

Garnett D. R., Dufour R. J., Peimbert M., Torres-Peimbert S., Shields G. A., Skillman E. D., Terlevich E., Terlevich R. J., 1995, Astrophys. J. Letters, 449, L77+

Guainazzi M., Matt G., Perola G. C., 2005, Astron. Astrophys., 444, 119

Hicks E. K. S., Davies R. I., Malkan M. A., Genzel R., Tacconi L. J., Müller Sánchez F., Sternberg A., 2009, Astrophys. J., 696, 448

Hollenbach D., McKee C. F., 1989, Astrophys. J., 342, 306

Izotov Y. I., Stasińska G., Meynet G., Guseva N. G., Thuan T. X., 2006, Astron. Astrophys., 448, 955

Jackson N., Beswick R. J., 2007, Mon. Not. R. Astron. Soc., 376, 719

Kewley L. J., Dopita M. A., Sutherland R. S., Heisler C. A., Trevena J., 2001, Astrophys. J., 556, 121

Knop R. A., Armus L., Matthews K., Murphy T. W., Soifer B. T., 2001, Astron. J., 122, 764

Krongold Y., Jiménez-Bailón E., Santos-Lleo M., Nicastro F., Elvis M., Brickhouse N., Andrade-Velazquez M., Binette L., Mathur S., 2009, Astrophys. J., 690, 773

Larkin J. E., Armus L., Knop R. A., Soifer B. T., Matthews K., 1998, Astrophys. J., Suppl. Ser., 114, 59

Longinotti A. L., Sim S. A., Nandra K., Cappi M., 2007, Mon. Not. R. Astron. Soc., 374, 237

Maloney P. R., Hollenbach D. J., Tielens A. G. G. M., 1996, Astrophys. J., 466, 561

McCall B. J., Huneycutt A. J., Saykally R. J., Geballe T. R., Djuric N., Dunn G. H., Semaniak J., Novotny O., Al-Khalili A., Ehlerding A., Hellberg F., Kalhori S., Neau A., Thomas R., Österdahl F., Larsson M., 2003, Nature, 422, 500

McGregor P. J., Hart J., Conroy P. G., Pfitzner M. L., Bloxham G. J., Jones D. J., Downing M. D., Dawson M., Young P., Jarnyk M., Van Harmelen J., 2003, in M. Iye & A. F. M. Moorwood ed., Society of Photo-Optical Instrumentation Engineers (SPIE) Conference Series Vol. 4841 of Society of Photo-Optical Instrumentation Engineers (SPIE) Conference Series, Gemini near-infrared integral field spectrograph (NIFS). pp 1581–1591

Meijerink R., Spaans M., Loenen A. F., van der Werf P. P., 2011, Astron. Astrophys., 525, A119+

Miller B. P., Brandt W. N., Schneider D. P., Gibson R. R., Steffen A. T., Wu J., 2011, Astrophys. J., 726, 20

Moshir M., Kopan G., Conrow T., McCallon H., Hacking P., Gregorich D., Rohrbach G., Melnyk M., Rice W., Fullmer L., White J., Chester T., 1990, in Bulletin of the American Astronomical Society Vol. 22 of Bulletin of the American Astronomical Society, The IRAS Faint Source Catalog, Version 2. pp 1325–+

Mould J. R., Huchra J. P., Freedman W. L., Kennicutt Jr. R. C., Ferrarese L., Ford H. C., Gibson B. K., Graham J. A., Hughes S. M. G., Illingworth G. D., Kelson D. D., Macri L. M., Madore B. F., Sakai S., Sebo K. M., Silbermann N. A., Stetson P. B., 2000, Astrophys. J., 529, 786

Mouri H., 1994, Astrophys. J., 427, 777

Mouri H., Kawara K., Taniguchi Y., 1993, Astrophys. J., 406, 52

Mouri H., Kawara K., Taniguchi Y., 2000, Astrophys. J., 528, 186

Mouri H., Nishida M., Taniguchi Y., Kawara K., 1990, Astrophys. J., 360, 55

Muñoz-Marín V. M., González Delgado R. M., Schmitt H. R., Cid Fernandes R., Pérez E., Storchi-Bergmann T., Heckman T., Leitherer C., 2007, Astron. J., 134, 648

Mulchaey J. S., Wilson A. S., Tsvetanov Z., 1996, Astrophys. J., 467, 197

Müller Sánchez F., Davies R. I., Genzel R., Tacconi L. J., Eisenhauer F., Hicks E. K. S., Friedrich S., Sternberg A., 2009, Astrophys. J., 691, 749

Oliva E., Marconi A., Maiolino R., Testi L., Mannucci F., Ghinassi F., Licandro J., Origlia L., Baffa C., Checcucci A., and 12 coauthors, 2001, Astron. Astrophys., 369, L5

Peimbert A., Peimbert M., 2010, Astrophys. J., 724, 791

Piconcelli E., Jimenez-Bailón E., Guainazzi M., Schartel N., Rodríguez-Pascual P. M., Santos-Lleó M., 2005, Astron. Astrophys., 432, 15

Quillen A. C., Alonso-Herrero A., Rieke M. J., Rieke G. H., Ruiz M., Kulkarni V., 1999, Astrophys. J., 527, 696

Ramos Almeida C., Pérez García A. M., Acosta-Pulido J. A., 2009, Astrophys. J., 694, 1379

Reunanen J., Kotilainen J. K., Prieto M. A., 2002, Mon. Not. R. Astron. Soc., 331, 154

Riffel R., Rodríguez-Ardila A., Pastoriza M. G., 2006, Astron. Astrophys., 457, 61

Riffel R. A., Storchi-Bergmann T., 2011a, Mon. Not. R. Astron. Soc., 411, 469

Riffel R. A., Storchi-Bergmann T., 2011b, Mon. Not. R. Astron. Soc., pp 1320–+

Riffel R. A., Storchi-Bergmann T., Dors O. L., Winge C., 2009, Mon. Not. R. Astron. Soc., 393, 783

Riffel R. A., Storchi-Bergmann T., Nagar N. M., 2010, Mon. Not. R. Astron. Soc., 404, 166

Riffel R. A., Storchi-Bergmann T., Winge C., Barbosa F. K. B., 2006, Mon. Not. R. Astron. Soc., 373, 2

Riffel R. A., Storchi-Bergmann T., Winge C., McGregor P. J., Beck T., Schmitt H., 2008, Mon. Not. R. Astron. Soc., 385, 1129

Rodríguez-Ardila A., Pastoriza M. G., Viegas S., Sigut T. A. A., Pradhan A. K., 2004, Astron. Astrophys., 425, 457

Rodríguez-Ardila A., Riffel R., Pastoriza M. G., 2005, Mon. Not. R. Astron. Soc., 364, 1041

Shaw G., Ferland G. J., Abel N. P., Stancil P. C., van Hoof P. A. M., 2005, Astrophys. J., 624, 794

Simpson C., Forbes D. A., Baker A. C., Ward M. J., 1996, Mon. Not. R. Astron. Soc., 283, 777

Skrutskie M. F., Cutri R. M., Stiening R., Weinberg M. D., Schneider S., Carpenter J. M., Beichman C., Capps R., Chester T., Elias J., and 21 coauthors, 2003, VizieR Online Data Catalog, 7233, 0

Storchi-Bergmann T., Lopes R. D. S., McGregor P. J., Riffel R. A., Beck T., Martini P., 2010, Mon. Not. R. Astron. Soc., 402, 819

Storchi-Bergmann T., McGregor P. J., Riffel R. A., Simões Lopes R., Beck T., Dopita M., 2009, Mon. Not. R. Astron. Soc., 394, 1148

Suchkov A., Allen R. J., Heckman T. M., 1993, Astrophys. J., 413, 542

Tananbaum H., Avni Y., Branduardi G., Elvis M., Fabbiano G., Feigelson E., Giacconi R., Henry J. P., Pye J. P., Soltan A., Zamorani G., 1979, Astrophys. J. Letters, 234, L9

Thompson Jr. R. J., 1995, Astrophys. J., 454, 660

Turner J. E. H., Allington-Smith J., Chapman S., Content R., Done C., Haynes R., Lee D., Morris S., 2002, Mon. Not. R. Astron. Soc., 331, 284

Veilleux S., Goodrich R. W., Hill G. J., 1997, Astrophys. J., 477, 631

Verner E. M., Verner D. A., Korista K. T., Ferguson J. W., Hamann F., Ferland G. J., 1999, Astrophys. J., Suppl. Ser., 120, 101

Zamorani G., Henry J. P., Maccacaro T., Tananbaum H., Soltan A., Avni Y., Liebert J., Stocke J., Strittmatter P. A., Weymann R. J., Smith M. G., Condon J. J., 1981, Astrophys. J., 245, 357